IEEE Access
Multidisciplinary ⋮ Rapid Review ⋮ Open Access Journal

Received 22 March 2023, accepted 10 April 2023, date of publication 18 April 2023, date of current version 24 April 2023.

Digital Object Identifier 10.1109/ACCESS.2023.3268133

RESEARCH ARTICLE

Intercomparison of the Averaged Induced Electric Field in Learning-Based Human Head Models Exposed to Low-Frequency Magnetic Fields

YINLIANG DIAO[1], (Member, IEEE), ESSAM A. RASHED[2], (Senior Member, IEEE), LUCA GIACCONE[3], (Senior Member, IEEE), ILKKA LAAKSO[4], (Member, IEEE), CONGSHENG LI[5], RICCARDO SCORRETTI[6,7], YOICHI SEKIBA[8], (Member, IEEE), KENICHI YAMAZAKI[9], (Senior Member, IEEE), AND AKIMASA HIRATA[10,11], (Fellow, IEEE)

[1]College of Electronic Engineering, South China Agricultural University, Guangzhou 510642, China
[2]Graduate School of Information Science, University of Hyogo, Kobe 650-0047, Japan
[3]Dipartimento Energia "G. Ferraris," Politecnico di Torino, 10129 Torino, Italy
[4]Department of Electrical Engineering and Automation, Aalto University, 02150 Espoo, Finland
[5]China Academy of Information and Communications Technology, Beijing 100191, China
[6]Ecole Centrale de Lyon, CNRS, INSA Lyon, Université Claude Bernard Lyon 1, University of Lyon, Ampère, UMR5005, 69622 Villeurbanne, France
[7]Department of Engineering, University of Perugia, 06125 Perugia, Italy
[8]Denryoku Computing Center Ltd., Tokyo 101-0054, Japan
[9]Central Research Institute of Electric Power Industry, Yokosuka 240-0196, Japan
[10]Department of Electrical and Mechanical Engineering, Nagoya Institute of Technology, Nagoya 466-8555, Japan
[11]Center of Biomedical Physics and Information Technology, Nagoya Institute of Technology, Nagoya 466-8555, Japan

Corresponding author: Yinliang Diao (diaoyinliang@ieee.org)

ABSTRACT Anatomical human models have been widely used in the assessment of induced field strength for low-frequency (LF) electromagnetic field exposure. One bottleneck is the assignment of a single electrical conductivity to all the voxels of the corresponding tissue. This simplification is known to cause computational artifact; therefore, a large reduction factor was considered in international guidelines and standards. Recently, head models with nonuniform conductivities generated using deep learning networks were proposed, and the effect on the reduction of staircasing artifacts was demonstrated. If the effectiveness of the models is confirmed for different models and codes, it would be useful to derive the relationship between the internal and external field strengths needed for setting the exposure limit. The Subcommittee 6 of the IEEE International Committee on Electromagnetic Safety Technical Committee 95 launched a working group to conduct the first intercomparison study of the induced electric field in learning-based head models exposed to LF magnetic fields. Seven international research groups have cooperated in this joint study. The highest relative difference (RD) in averaged electric fields was 23%, which is attributable to the difference caused the by scalar potential finite difference (SPFD) method and finite element method. Except for one group, the RDs in the 100th and 99th percentile values of the averaged electric field using the SPFD method with different solvers and codes were below 1%, indicating that the uncertainty due to different codes is sufficiently small under the same exposure scenarios. The findings would be informative for future revision of exposure limits and reduction factors in the exposure standard, which is closely related to computational uncertainty.

INDEX TERMS Low frequency, electromagnetic safety, human protection, standardization.

I. INTRODUCTION

Human safety from electromagnetic field exposure has been a long-standing concern for the public. To protect humans from the dangers of electromagnetic field exposure, the

The associate editor coordinating the review of this manuscript and approving it for publication was Mohammed Bait-Suwailam.

IEEE International Commission of Electromagnetic Safety (ICES) and the International Commission on Non-ionizing Radiation Protection (ICNIRP) published standards [1] and guidelines [2], [3] for setting up exposure limits. These standards and guidelines are periodically revised to reflect the latest scientific knowledge in the understanding of the health effects, dosimetry, etc.

The established effects and the lowest threshold identified in the IEEE standards and ICNIRP guidelines in the low-frequency (LF) range were central nervous system stimulation at <300–400 Hz and peripheral nervous system stimulation at <100 kHz, respectively [1], [3]. Two metric types have been developed. The first is the basic restriction in the ICNIRP guidelines (called the dosimetric reference limit in the IEEE standards), defined in terms of the spatially averaged induced internal electric field strength, derived from the threshold of adverse effects considering the reduction (safety) factor [3]. The second is the reference level in the ICNIRP guidelines (called exposure reference level in the IEEE standards). The latter is defined as external electric or magnetic field strength for facilitating compliance assessment.

External electric or magnetic field is derived from the limit of induced electric field strength in a conservative manner. The IEEE used homogeneous ellipses with different dimensions for each body part with analytical solutions [1], whereas the ICNIRP used an anatomical human body model using numerical computations [4].

In the ICNIRP guidelines 2010 [3], due to computational uncertainty, an additional reduction factor of 3 was considered in the limit derivation, whereas the rationale was not explicitly mentioned. Note that such a reduction factor associated with the computation is not applied to radiofrequency guidelines. If the uncertainty associated with the dosimetry is quantified, it would facilitate the setting of an appropriate reduction factor and limits in a more robust manner [5]. Therefore, continuous improvement in computational models and methods is critical to the establishment of the scientific basis for exposure standards [6], [7].

Traditional voxel models were developed by performing segmentation of medical images into various tissues and then assigning the corresponding tissue with dielectric properties (electrical conductivity in LF) acquired from literatures [8], [9]. Although many dosimetry studies have used voxel-based human models [4], [10], [11], [12], [13], [14], [15], [16], [17], [18], [19], [20], [21], [22], [23], [24], [25], an important issue with the use of such models in the exposure criteria is the numerical artifacts, specifically the staircasing error inherent to voxel models [26], [27]. This is a result of tissue digitization as a set of voxels that enables hard transition of electrical conductivity across curved tissue interfaces. To resolve the issue of computational uncertainties [7], intercomparisons have been previously conducted for computations using voxel models [28], [29], [30] due to the lack of exact solution.

Recently, head models with nonuniform conductivity have been developed and utilized for dosimetry [31], [32]. In [31], head models with smoothly changing conductivities within the same tissue were directly constructed from T1-/T2-weighted magnetic resonance images (MRIs) using a deep learning network. Although it is nearly impossible to verify the process for the reconstructed dielectric properties using deep learning methods in most cases, previous studies have demonstrated some advantages, such as the following: 1) smooth transition of conductivity values is more reasonable for biological media, reducing staircasing errors in voxel-based computation of the induced fields; 2) it reflects the internal changes in dielectric properties within a specific tissue [9].

Research needs on the intercomparison and tissue conductivity assignment are listed in the research agenda published by international standardization bodies [6], [7]. To resolve these issues, the Subcommittee 6 of IEEE ICES Technical Committee 95 launched a working group on a novel modeling technique for LF dosimetry. One goal of the working group is to conduct intercomparison studies using these novel learning-based models to provide scientific data used for deriving the exposure limits. Seven groups from organizations worldwide participated in this intercomparison study. Five human head models were developed using CondNet [31] and shared to all participants. Induced electric fields were computed by each group using their own developed computational codes. The averaged electric field in the skin, gray matter (GM), and white matter (WM) was reported for the comparison. To the best of our knowledge, this is the first study that conducted an intercomparison using novel learning-based head models for the assessment of LF magnetic field exposures. The findings of this study would be useful for setting the exposure limits and reduction factors in future revisions of the electromagnetic exposure standard.

II. MODELS AND METHODS

A. MODELS

MRIs of five subjects from the Brain Multimodality Dataset [33] were used to develop voxel-based head models with a resolution of 1 mm × 1 mm × 1 mm. CondNet [31] was used for the automatic generation of the nonuniform models. CondNet is a deep learning convolutional neural network that enables the estimation of voxel dielectric properties, such as conductivity and permittivity, directly from MRI scans without segmentation. The network is designed to map the input anatomical images to conductivity maps of the human head. The network is trained using a standard data processing pipeline that considers the segmentation of several subjects to generate a training dataset, and then new subjects can be directly developed from MRI scans. In TABLE 1, the tissue conductivities used for training the network are listed [8]. In addition, the skin, GM, and WM of the five models were segmented using ForkNet [34] to identify the field inside each tissue for result evaluation and comparison.

Fig. 1 presents an axial cross-sectional slice of the conductivity distributions of the five non-uniform head models at 50 Hz and 10 kHz, where smooth transition across the tissue interfaces can be observed. Fig. 2 presents the statistic distributions of the conductivity of the WM of the five learning-based nonuniform head models. As can be seen from Fig. 2, within the same WM tissue, the conductivity values are different across the subjects, which is a result of the different gray levels of the medical images of subjects, reflecting the variability in the tissue conductivity values of subjects.

TABLE 1. The conductivities (s/m) of the major tissues used for training condNet.

Tissue	50 Hz	10 kHz
Blood	0.70	0.70
Cancellous Bone	0.08	0.08
Cortical Bone	0.02	0.02
Cerebrospinal Fluid (CSF)	2.0	2.0
Cerebellum	0.095	0.13
Fat	0.04	0.04
Muscle	0.23	0.34
Skin	0.1	0.1
Grey Matter (GM)	0.075	0.1
White Matter (WM)	0.053	0.07

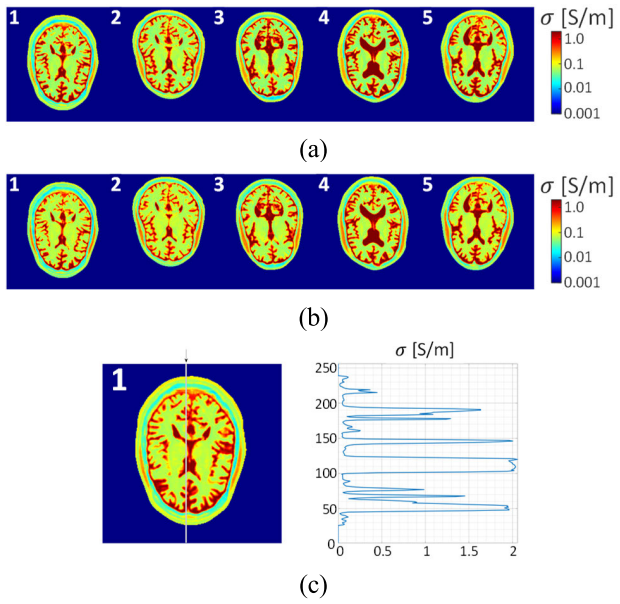

FIGURE 1. Distributions of the conductivity on the cross sections of five non-uniform head models at (a) 50 Hz and (b) 10 kHz. Conductivity plotted along a line for model no. 1, highlighting the nonuniformity and smooth transitions (c).

B. EXPOSURE SCENARIO

Uniform magnetic fields of 200 μT at 50 Hz and 27 μT at 10 kHz were considered, corresponding to the reference levels in the ICNIRP guidelines for the general public. The direction of the magnetic field was aligned with the TOP direction

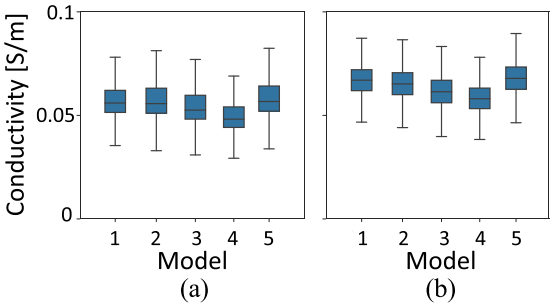

FIGURE 2. Boxplots of the WM conductivities at (a) 50 Hz and (b) 10 kHz for different head models.

(from top to bottom) due to the largest cross-sectional area in the axial plane of the truncated heads. For this intercomparison study, the averaged induced electric fields in the skin, GM, and WM were computed and reported.

C. LF ELECTROMAGNETIC COMPUTATIONAL METHODS

The induced electric fields in the voxel-based anatomical models are numerically solved. At frequencies below 10 MHz, the human body is assumed not to perturb the external magnetic field [35]. In this frequency range, the conduction current completely dominates the displacement current $\sigma \gg \omega\epsilon$, and thus, Maxwell's equations can be simplified with a quasistatic approximation [35], [36], [37] by ignoring the displacement current. Thus, the tissue permittivity can be neglected for the LF electromagnetic computation.

The scalar potential finite difference (SPFD) method was widely adopted to solve the quasistatic magnetic field exposure problem. The SPFD method sets the branch current instead of the loop current. The unknowns in this method are the scalar potentials ϕ at the nodes (vertex) of the voxel. The scalar potentials ϕ for an external magnetic field were determined using the following equation:

$$\nabla \cdot [\sigma\,(-\nabla\phi - j\omega \boldsymbol{A}_0)] = 0, \tag{1}$$

where $\boldsymbol{A}_0$ and σ denote the magnetic vector potential of the applied magnetic field and the tissue conductivity, respectively, and ω denotes the angular frequency. The potential ϕ was subsequently solved numerically. The electric field along the side of the voxel is obtained as follows:

$$\boldsymbol{E} = -\nabla\phi - j\omega \boldsymbol{A}_0, \tag{2}$$

In the case of scalar potential finite element method (FEM), Equation (1) is written in a weak form before being discretized [38]. Hence, the obtained linear system is different from that obtained using the SPFD method.

The SPFD method was employed by groups from the China Academy of Information and Communications Technology (CAICT), Central Research Institute of Electric Power Industry (CRIEPI), Nagoya Institute of Technology (NITech), and South China Agricultural University (SCAU). Politecnico di Torino (PoliTO) also adopted the SPFD, but the formulation was based on algebraic framework [39], [40]. The FEM was

used by groups from Aalto University and CNRS/University of Perugia (Ampère). The scalar potential was discretized on hexahedra corresponding to voxels by using classical trilinear nodal shape functions. The matrix equations for the SPFD method at NITech and for the FEM at Aalto University were iteratively solved using the geometric multigrid method with successive over-relaxation smoothing [41]. The biconjugate gradient stabilized method was employed by the CRIEPI, and the Jacobi iterative method with GPU acceleration was adopted by the SCAU. The algebraic multigrid method combined with the induced dimension reduction method was employed by the CAICT to solve the sparse linear system. The aggregation-based algebraic multigrid solver AGMG [40] was used by PoliTO and Ampère. The stop criterion of relative residual $<10^{-6}$ or lower was used by all groups.

D. SPATIAL AVERAGING OF THE INDUCED ELECTRIC FIELDS

Both the ICNIRP guidelines and the IEEE standard use a spatially averaged induced electric field as a metric to protect humans from exposure to LF field. This is related to the prevention of nerve stimulation in the peripheral and nervous systems. The ICNIRP guidelines 2010 [3] used an averaging volume of 8-mm^3 (2 mm $\times$ 2 mm $\times$ 2 mm) cube together with the 99$^{\text{th}}$ percentile for the induced electric field in a targeted tissue as the relevant dosimetric quantity [3]. The IEEE standard prescribed the induced electric field to be averaged over a 5-mm line segment [1]. A previous study [42] developed detailed schemes for these averaging methods and demonstrated that both are comparable. This study used a cubically averaged electric field as a metric for comparison. As presented in Fig. 3 and (3), the volume-averaged electric field, $\bar{E}_{i,j,k}$, for voxel at (i, j, k) was evaluated as the arithmetic average of the vector electric field in the 8-mm^3 cube.

$$\bar{E}_{i,j,k} = \left\| \sum_{x=i-1}^{i+1} \sum_{y=j-1}^{j+1} \sum_{z=k-1}^{k+1} w_{x,y,z} \boldsymbol{E}_{x,y,z} \right\|, \tag{3}$$

where w denotes the weight for voxel at (x, y, z). The weights of the voxels that intersected with the 8-mm^3 cube were determined based on the fraction of the intersected volume.

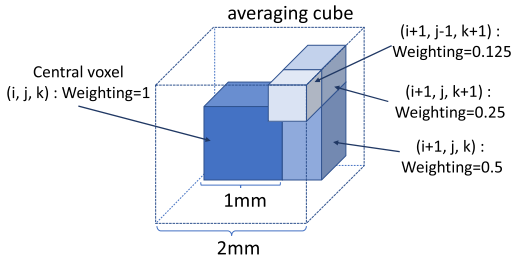

FIGURE 3. Demonstration of the cubic averaging method.

Two cubic averaging methods were considered depending on the inclusion of nontarget tissues: in method 1, all types of tissues are allowed in the averaging cube, and averaging is performed over all voxels in the cube. In method 2, only the target tissue is allowed in the cube. If the averaging cube contains voxels belonging to other tissues, the averaging will not be performed, and these voxels are excluded from the computations of the percentile values. In TABLE 2, the models and computational parameters adopted by seven groups for the comparison of the results are presented.

TABLE 2. Summary of the models and parameters for inter comparison.

Model no.:	1, 2, 3, 4, and 5
Target tissue:	Skin, GM, and WM
Frequency:	50 Hz and 10 kHz
Cubic averaging method:	Methods 1 and 2
Percentile:	99$^{\text{th}}$ and 100$^{\text{th}}$ percentile (maximum) values

For the intercomparison of the results, the relative difference (RD) in percentage between the reported results and a reference value were calculated as follows:

$$RD = \left| \frac{A_i - A_r}{A_r} \right| \times 100, \tag{4}$$

where A_i denotes the results obtained by the i^{th} group, and A_r denotes the reference value, which is the mean of the results obtained by all seven research group.

III. RESULTS

A. ELECTRIC FIELD DISTRIBUTIONS IN THE HEAD MODELS

The electric field distributions on the cross sections of head model no. 1 computed by seven research groups are presented in Fig. 4. The electric field distributions agree well with each other. In Fig. 5, the electric field distributions on the cross sections of the five head models are presented. Due to the similarity, the data reported from one group are presented. Figs. 5 (a) and (b) present the electric field distributions in all tissues and those in the GM and WM of the head models. In Fig. 5 (b), the GMs are masked by translucent shaders for clarity. As can be seen, staircasing artifacts have been validly suppressed in the nonuniform head models compared with the previous results obtained using segmented head models [25], [43], [44], [45]. On the cross sections, the highest electric field strength mostly appears in the gyruses of the WM due to the higher conductivity of the outermost layers of the GM voxels because of the effect of the neighboring high-conductivity CSF for the learning-based models.

B. INTERCOMPARISON OF THE PERCENTILE VALUES

The means and RDs of the 100$^{\text{th}}$ percentile values of the averaged electric fields from the seven groups using methods 1 and 2 are presented in TABLES 3 and 4, respectively. For method 1, the highest mean values of 100$^{\text{th}}$ percentile values at 50 Hz are 8.09 and 9.00 mV/m in GM and WM, respectively. For method 2, the highest 100$^{\text{th}}$ percentile values at 50 Hz are 6.88 and 8.67 mV/m in GM and WM, respectively.

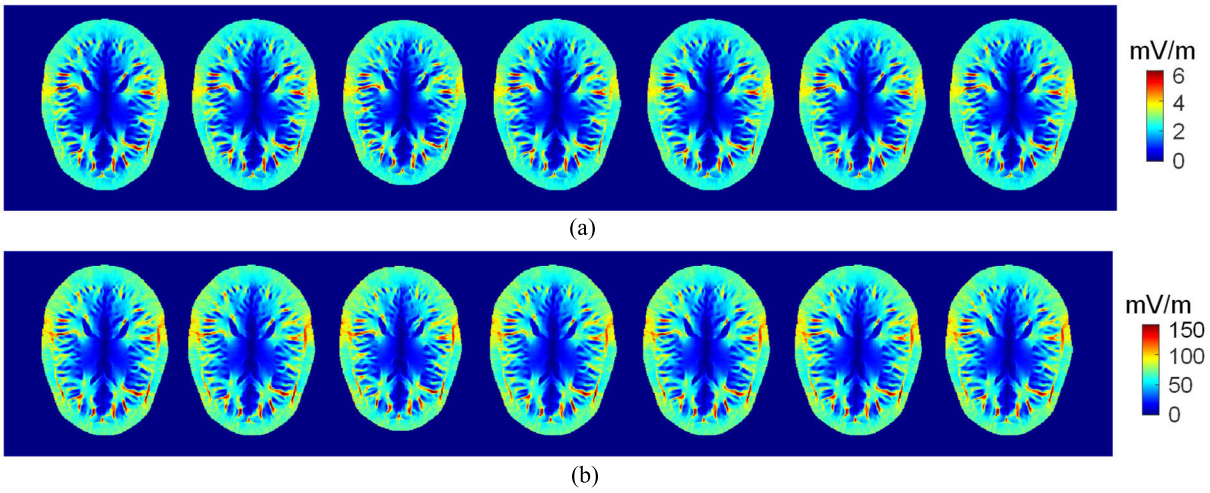

FIGURE 4. Comparison of the electric field distributions for model no. 1 at (a) 50 Hz and (b) 10 kHz. From left to right are results computed by groups from Aalto, Ampère, CAICT, CRIEPI, NITech, PoliTO, and SCAU.

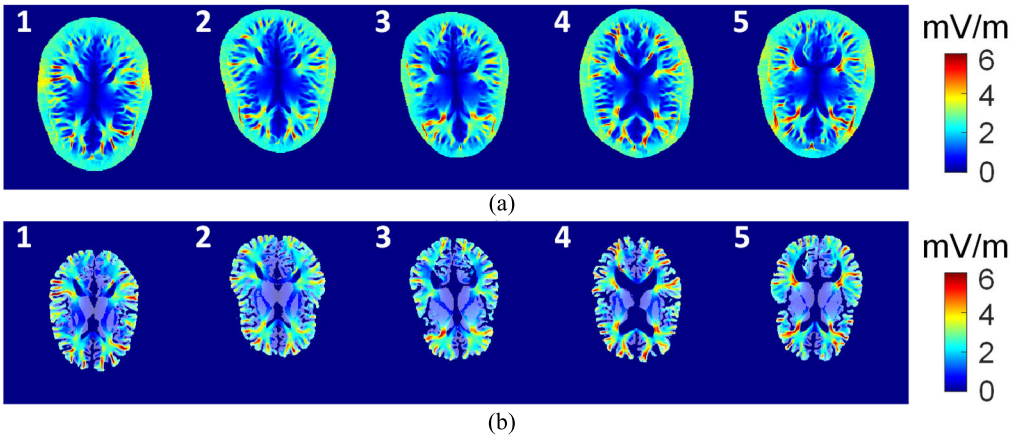

FIGURE 5. Distributions of the electric field strengths in (a) all tissues and (b) GM and WM of the head models at 50 Hz. The GMs in (b) are masked by translucent shaders.

For method 1, the highest mean values of 99th percentile values are 4.20 and 5.03 mV/m in GM and WM, respectively, as presented in TABLE 5. For method 2, the 99th percentile values are 4.11 and 4.67 mV/m in GM and WM, respectively, as presented in TABLE 6.

At 10 kHz, the highest mean values of 100th percentile values are 191 and 207 mV/m in GM and WM for method 1, respectively. For method 2, the highest 100th percentile values are 160 and 197 mV/m in GM and WM, respectively. The 99th percentile values obtained using method 1 are 109 and 124 mV/m in GM and WM, respectively, and the 99th percentile values are 108 mV/m in GM and 112 mV/m in WM for method 2.

The RD results show close agreement with the computational results across the seven groups. The highest RD is 23% in the results obtained using FEM. Except for the results from two groups, the RDs are below 1% in most cases. For the 100th percentile of the averaged electric field using method 1, the maximum RDs are about 15%, 23%, and 5% for GM, WM, and skin, respectively. For method 2, the highest RDs are about 4%, 9%, and 14% for GM, WM, and skin, respectively. This is attributable to the definition of method 2 that excludes voxels where other nontarget tissues are included in the averaging volume.

As expected, the RDs for the 99th percentile values of the cubically averaged electric field strength are globally lower than those for the 100th percentile values. For the electric field averaged using method 1, the maximum RDs are 23% and 11% for the 100th and 99th percentile values, respectively. For the electric field averaged using method 2, the maximum RDs are 14% and 7% for the 100th and 99th percentile values, respectively. Except for the results from one group, the highest RD in the 99th percentile values computed using method 2 are generally below 1%. This may be attributable to the different interpretation of the cubic averaging scheme.

The computed electric fields are in excellent agreement for groups using the SPFD method with their individual solvers, except for one group, whose RDs are well below 1%. Slightly

TABLE 3. Inter-comparison of the 100th percentile (maximum) value of the electric field in five head models using method 1, the percent values are RD.

Tissue	Freq	Model	Mean [mV/m]	Aalto	Ampère	CAICT	CRIEPI	NITech	PoliTO	SCAU
GM	50 Hz	1	7.08	4.96%	15.24%	0.59%	2.42%	2.42%	2.42%	2.42%
		2	6.04	2.21%	3.27%	5.65%	1.68%	1.68%	1.68%	1.68%
		3	7.16	1.25%	7.73%	7.45%	0.38%	0.38%	0.38%	0.39%
		4	8.09	3.94%	5.21%	5.75%	1.76%	1.76%	1.76%	1.74%
		5	7.12	1.99%	4.13%	6.51%	0.09%	0.09%	0.09%	0.11%
	10 kHz	1	161	2.04%	1.90%	4.90%	0.24%	0.24%	0.24%	0.24%
		2	163	2.90%	4.92%	7.43%	2.37%	2.37%	2.37%	2.36%
		3	185	2.43%	0.60%	7.27%	1.06%	1.06%	1.06%	1.07%
		4	188	3.55%	2.58%	5.93%	1.25%	1.25%	1.25%	1.23%
		5	191	3.18%	4.31%	6.06%	1.80%	1.80%	1.80%	1.78%
WM	50 Hz	1	8.64	1.00%	9.56%	5.43%	1.28%	1.28%	1.28%	1.29%
		2	7.11	0.99%	11.32%	9.96%	0.59%	0.59%	0.59%	0.59%
		3	7.77	1.73%	11.72%	13.94%	0.12%	0.12%	0.12%	0.13%
		4	9.00	0.08%	22.77%	12.60%	2.56%	2.56%	2.56%	2.57%
		5	8.10	0.68%	19.16%	11.68%	2.04%	2.04%	2.04%	2.05%
	10 kHz	1	190	2.54%	7.19%	11.33%	0.40%	0.40%	0.40%	0.40%
		2	177	1.41%	7.43%	10.24%	0.35%	0.35%	0.35%	0.35%
		3	195	2.16%	9.44%	14.46%	0.71%	0.71%	0.71%	0.72%
		4	207	1.21%	12.72%	11.66%	0.56%	0.56%	0.56%	0.58%
		5	200	1.46%	8.02%	9.86%	0.10%	0.10%	0.10%	0.08%
Skin	50 Hz	1	7.93	1.48%	1.47%	4.59%	0.41%	0.41%	0.41%	0.42%
		2	7.87	0.05%	0.04%	0.67%	0.15%	0.15%	0.15%	0.14%
		3	7.74	0.93%	0.92%	0.12%	0.49%	0.49%	0.49%	0.50%
		4	8.55	0.29%	0.28%	0.10%	0.12%	0.12%	0.12%	0.11%
		5	8.70	0.34%	0.34%	0.59%	0.02%	0.02%	0.02%	0.03%
	10 kHz	1	228	0.59%	0.59%	0.28%	0.36%	0.36%	0.36%	0.37%
		2	222	0.21%	0.21%	0.73%	0.08%	0.08%	0.08%	0.08%
		3	198	0.91%	0.91%	0.01%	0.46%	0.46%	0.46%	0.47%
		4	257	0.51%	0.52%	0.25%	0.20%	0.20%	0.20%	0.19%
		5	245	0.21%	0.20%	0.75%	0.29%	0.29%	0.29%	0.28%

TABLE 4. Inter-comparison of the 100th percentile (maximum) value of the electric field in five head models using method 2.

Tissue	Freq	Model	Mean [mV/m]	Aalto	Ampère	CAICT	CRIEPI	NITech	PoliTO	SCAU
GM	50 Hz	1	5.89	0.72%	0.71%	0.19%	0.41%	0.41%	0.41%	0.40%
		2	5.77	1.24%	1.24%	4.11%	0.40%	0.40%	0.40%	0.42%
		3	6.35	1.00%	1.00%	0.62%	0.35%	0.35%	0.35%	0.34%
		4	6.88	2.92%	2.93%	1.24%	1.16%	1.16%	1.16%	1.14%
		5	5.48	1.34%	1.34%	0.37%	0.58%	0.58%	0.58%	0.56%
	10 kHz	1	153	1.22%	1.20%	0.79%	0.41%	0.41%	0.41%	0.40%
		2	146	1.22%	1.22%	3.43%	0.25%	0.25%	0.25%	0.25%
		3	156	0.54%	0.55%	0.19%	0.23%	0.23%	0.23%	0.23%
		4	160	1.95%	1.96%	1.08%	0.71%	0.71%	0.71%	0.69%
		5	139	0.90%	0.90%	0.04%	0.44%	0.44%	0.44%	0.42%
WM	50 Hz	1	7.52	1.79%	1.78%	3.40%	0.04%	0.04%	0.04%	0.05%
		2	6.22	0.82%	0.82%	3.11%	0.37%	0.37%	0.37%	0.37%
		3	6.54	1.12%	1.11%	5.00%	0.70%	0.70%	0.70%	0.68%
		4	8.67	1.74%	1.72%	5.64%	0.55%	0.55%	0.55%	0.53%
		5	7.28	0.66%	0.66%	3.64%	0.58%	0.58%	0.58%	0.57%
	10 kHz	1	176	2.60%	2.58%	8.94%	0.94%	0.94%	0.94%	0.94%
		2	142	0.30%	0.30%	1.78%	0.30%	0.30%	0.30%	0.30%
		3	160	0.74%	0.72%	4.12%	0.67%	0.67%	0.67%	0.66%
		4	197	1.73%	1.71%	6.00%	0.64%	0.64%	0.64%	0.62%
		5	161	0.44%	0.41%	0.30%	0.13%	0.13%	0.13%	0.15%
Skin	50 Hz	1	6.94	2.55%	2.55%	2.89%	0.56%	0.56%	0.56%	0.54%
		2	5.79	3.69%	3.69%	14.29%	1.72%	1.72%	1.72%	1.73%
		3	6.54	2.10%	2.10%	4.35%	0.04%	0.04%	0.04%	0.03%
		4	7.75	0.08%	0.08%	1.65%	0.45%	0.45%	0.45%	0.44%
		5	6.70	1.34%	1.33%	3.41%	0.19%	0.19%	0.19%	0.18%
	10 kHz	1	183	2.59%	2.59%	7.31%	0.53%	0.53%	0.53%	0.53%
		2	164	3.37%	3.38%	11.63%	1.22%	1.22%	1.22%	1.22%
		3	165	2.01%	2.01%	4.41%	0.10%	0.10%	0.10%	0.09%
		4	237	0.05%	0.05%	1.00%	0.28%	0.28%	0.28%	0.27%
		5	189	0.03%	0.03%	1.31%	0.35%	0.35%	0.35%	0.33%

TABLE 5. Inter-comparison of the 99th percentile value of the electric field in five head models using method 1.

Tissue	Freq	Model	Mean [mV/m]	Aalto	Ampère	CAICT	CRIEPI	NITech	PoliTO	SCAU
GM	50 Hz	1	3.74	1.46%	1.62%	2.56%	0.68%	0.68%	0.68%	0.69%
		2	3.53	1.62%	0.99%	3.53%	0.72%	0.73%	0.73%	0.73%
		3	3.95	1.48%	0.92%	4.25%	0.46%	0.47%	0.47%	0.47%
		4	4.20	1.91%	0.25%	4.84%	0.79%	0.80%	0.80%	0.78%
		5	3.83	1.66%	0.78%	3.48%	0.65%	0.65%	0.65%	0.66%
	10 kHz	1	99	1.48%	0.46%	4.33%	0.83%	0.83%	0.83%	0.82%
		2	93	1.47%	0.09%	4.38%	0.70%	0.71%	0.71%	0.70%
		3	103	1.37%	1.57%	5.12%	0.54%	0.54%	0.54%	0.55%
		4	109	1.66%	0.43%	5.27%	0.79%	0.80%	0.79%	0.79%
		5	101	1.58%	0.62%	5.30%	0.77%	0.77%	0.77%	0.78%
WM	50 Hz	1	4.66	0.97%	6.79%	8.98%	0.30%	0.30%	0.30%	0.31%
		2	4.32	1.34%	6.38%	10.74%	0.75%	0.76%	0.76%	0.76%
		3	4.64	1.43%	3.92%	10.07%	1.18%	1.18%	1.18%	1.18%
		4	5.03	1.22%	5.79%	9.86%	0.71%	0.72%	0.71%	0.71%
		5	4.90	1.11%	5.41%	9.33%	0.70%	0.70%	0.70%	0.70%
	10 kHz	1	114	1.32%	5.53%	10.78%	0.98%	0.98%	0.98%	0.98%
		2	105	1.34%	5.25%	10.11%	0.88%	0.88%	0.88%	0.88%
		3	114	1.43%	3.66%	10.26%	1.29%	1.29%	1.29%	1.29%
		4	124	1.20%	5.09%	9.74%	0.86%	0.86%	0.86%	0.87%
		5	119	1.28%	4.89%	9.70%	0.88%	0.88%	0.88%	0.88%
Skin	50 Hz	1	4.33	1.55%	1.47%	8.91%	1.47%	1.47%	1.47%	1.47%
		2	4.06	0.77%	1.01%	5.27%	0.87%	0.87%	0.87%	0.87%
		3	3.72	1.37%	0.69%	4.85%	0.69%	0.70%	0.70%	0.70%
		4	4.21	1.30%	0.84%	5.94%	0.94%	0.95%	0.95%	0.96%
		5	4.09	0.89%	0.94%	4.78%	0.74%	0.74%	0.74%	0.74%
	10 kHz	1	121	0.99%	0.99%	5.89%	0.97%	0.98%	0.98%	0.98%
		2	113	0.73%	0.87%	4.95%	0.83%	0.84%	0.84%	0.85%
		3	101	1.29%	0.86%	4.98%	0.70%	0.71%	0.71%	0.71%
		4	115	1.20%	0.87%	5.81%	0.93%	0.93%	0.93%	0.94%
		5	112	0.83%	0.92%	4.79%	0.76%	0.76%	0.76%	0.76%

TABLE 6. Inter-comparison of the 99.

Tissue	Freq	Model	Mean [mV/m]	Aalto	Ampère	CAICT	CRIEPI	NITech	PoliTO	SCAU
GM	50 Hz	1	3.55	0.73%	0.72%	2.08%	0.15%	0.16%	0.16%	0.16%
		2	3.36	0.87%	0.88%	2.12%	0.08%	0.10%	0.09%	0.10%
		3	3.34	0.74%	0.72%	0.10%	0.34%	0.34%	0.34%	0.33%
		4	4.11	1.31%	1.29%	3.28%	0.17%	0.17%	0.17%	0.17%
		5	3.49	0.68%	0.64%	1.12%	0.09%	0.03%	0.03%	0.05%
	10 kHz	1	93	0.78%	0.77%	1.81%	0.05%	0.07%	0.07%	0.06%
		2	89	0.91%	0.89%	2.78%	0.23%	0.25%	0.25%	0.25%
		3	90	0.58%	0.56%	0.73%	0.11%	0.10%	0.10%	0.09%
		4	108	1.18%	1.16%	4.43%	0.51%	0.53%	0.53%	0.52%
		5	93	0.98%	0.95%	2.58%	0.12%	0.18%	0.18%	0.17%
WM	50 Hz	1	4.08	0.57%	0.56%	3.92%	0.69%	0.70%	0.70%	0.69%
		2	3.91	0.96%	0.94%	5.91%	0.99%	1.01%	1.00%	1.01%
		3	4.39	1.10%	1.10%	7.38%	1.29%	1.30%	1.30%	1.30%
		4	4.54	0.74%	0.72%	5.33%	0.97%	0.97%	0.97%	0.96%
		5	4.67	0.94%	0.92%	6.81%	1.24%	1.24%	1.24%	1.23%
	10 kHz	1	100	0.70%	0.68%	4.99%	0.89%	0.91%	0.90%	0.90%
		2	94	0.80%	0.81%	4.94%	0.83%	0.84%	0.84%	0.83%
		3	107	0.99%	0.97%	7.14%	1.29%	1.30%	1.30%	1.30%
		4	112	0.80%	0.80%	5.52%	0.98%	0.98%	0.98%	0.99%
		5	111	0.87%	0.85%	5.89%	1.04%	1.05%	1.05%	1.04%
Skin	50 Hz	1	4.10	1.27%	1.28%	6.92%	1.09%	1.09%	1.09%	1.09%
		2	3.89	0.59%	0.61%	3.26%	0.50%	0.53%	0.51%	0.51%
		3	3.66	0.97%	0.98%	4.70%	0.67%	0.72%	0.68%	0.67%
		4	4.01	0.77%	0.75%	4.49%	0.73%	0.75%	0.75%	0.74%
		5	3.92	0.62%	0.62%	2.92%	0.42%	0.43%	0.42%	0.42%
	10 kHz	1	114	0.66%	0.65%	3.57%	0.54%	0.58%	0.58%	0.56%
		2	110	0.56%	0.56%	3.97%	0.71%	0.72%	0.71%	0.71%
		3	98	0.87%	0.86%	4.14%	0.59%	0.61%	0.61%	0.60%
		4	109	0.75%	0.74%	4.35%	0.71%	0.72%	0.72%	0.72%
		5	108	0.70%	0.70%	3.32%	0.47%	0.49%	0.48%	0.47%

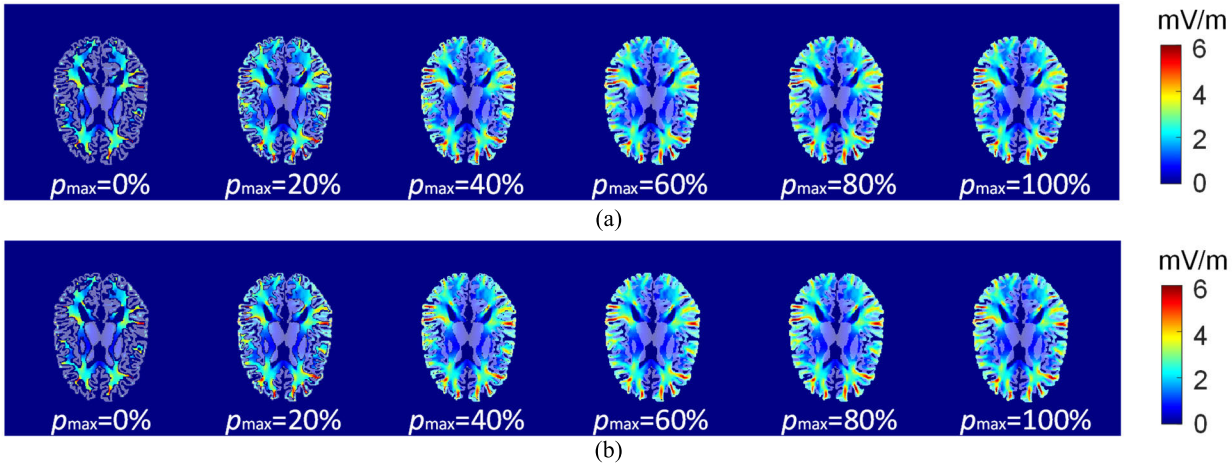

FIGURE 6. Distributions of the averaged electric field in GM and WM of model no. 1 for (a) method 1 and (b) method 2 for various pmax at 50 Hz. The GMs are masked by translucent shaders.

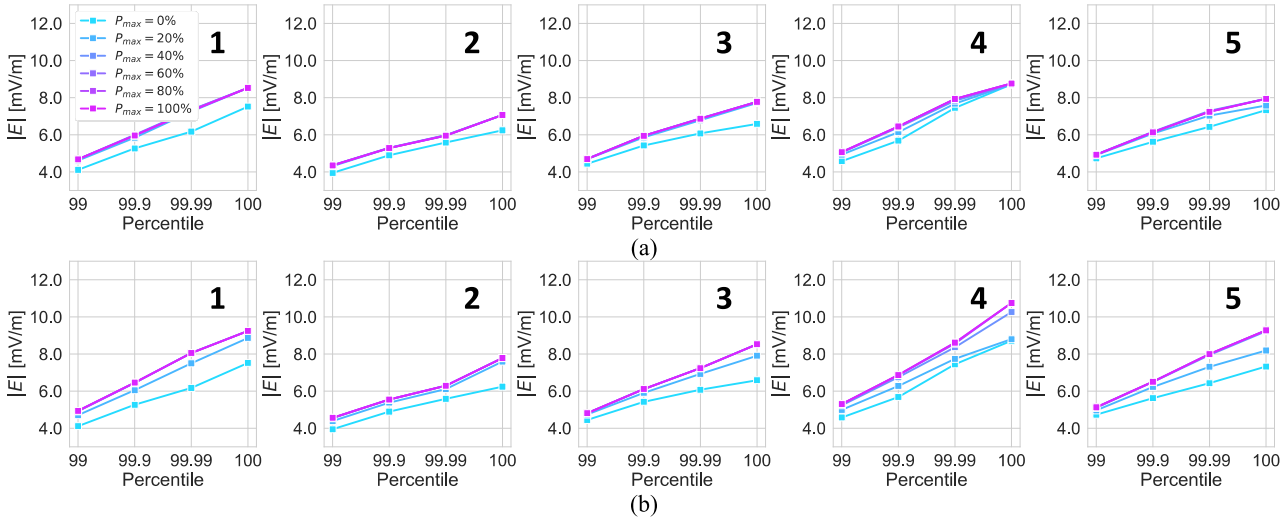

FIGURE 7. Percentile values of averaged electric field strengths using (a) method 1 and (b) method 2 in WM for varying pmax values at 50 Hz.

higher RDs were observed in the electric field computed between using the SPFD method and FEM. This is mainly attributable to the differences in the nodal schemes. Higher RDs are observed in GM and WM using method 1. For method 2, as the number of excluded voxels is high, the RDs are below 4%. Furthermore, the results computed using FEM in this study usually exhibit higher electric field strengths than the SPFD method [38].

C. EFFECT OF THE INCLUSION RATIO OF THE NONTARGET TISSUE IN THE AVERAGING VOLUME

For method 1, as all tissues can be included in the averaging volume, the averaged electric field is affected by the electric field strengths in neighboring nontarget tissues. While for method 2, because only the target tissue is allowed in the cube, the number of voxels where averaging is not performed becomes larger. Here, we considered the effect of the maximum permissible percentage of other tissues inside the averaging cube on the averaged electric field, $p_{\max}$, in the averaged electric fields defined as follows:

$$\bar{E}_{i,j,k} = \begin{cases} \left\| \sum_{x=i-1}^{i+1} \sum_{y=j-1}^{j+1} \sum_{z=k-1}^{k+1} w_{x,y,z} \boldsymbol{E}_{x,y,z} \right\|, & \text{if } p \le p_{\max} \\ 0, & \text{otherwise} \end{cases} \tag{5}$$

where p denotes the volume percentage of other nontarget tissues inside the 8-mm^3 cube, and $p_{\max}$ denotes the maximum permissible percentage of nontarget tissues in the cube. If $p > p_{\max}$, averaging will not be performed, and that voxel will be excluded from the computation of percentile values. Two averaging methods were considered. For method 1, averaging was performed over all voxels in the cube. For method 2, averaging was performed over the voxels of the target tissue in the cube. The averaged electric fields were

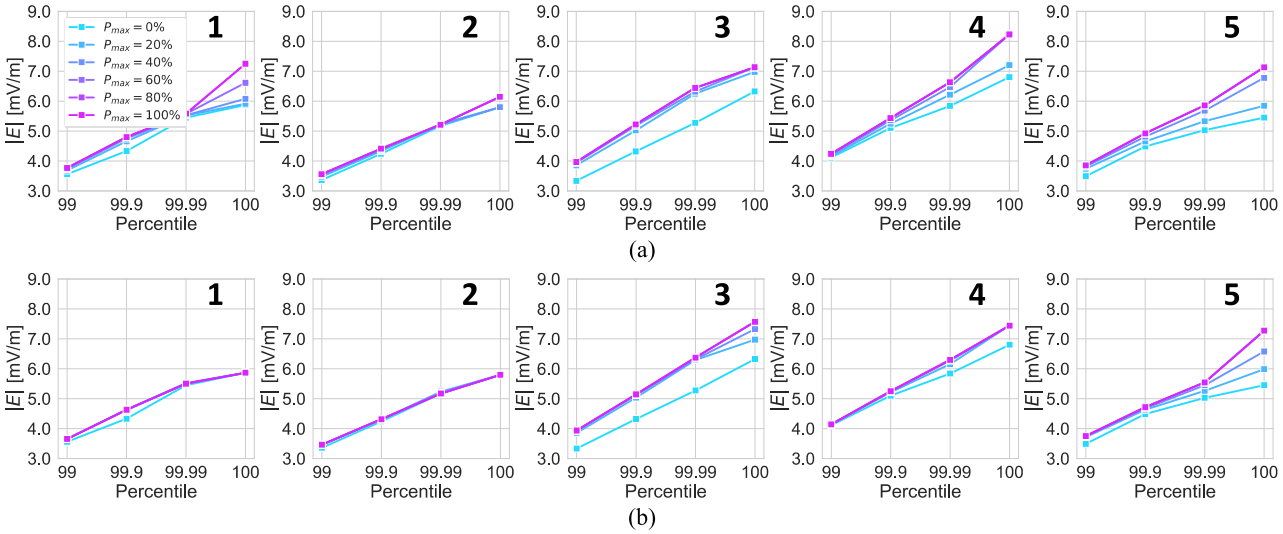

FIGURE 8. Percentile values of averaged electric field strengths using (a) method 1 and (b) method 2 in GM for varying pmax values at 50 Hz.

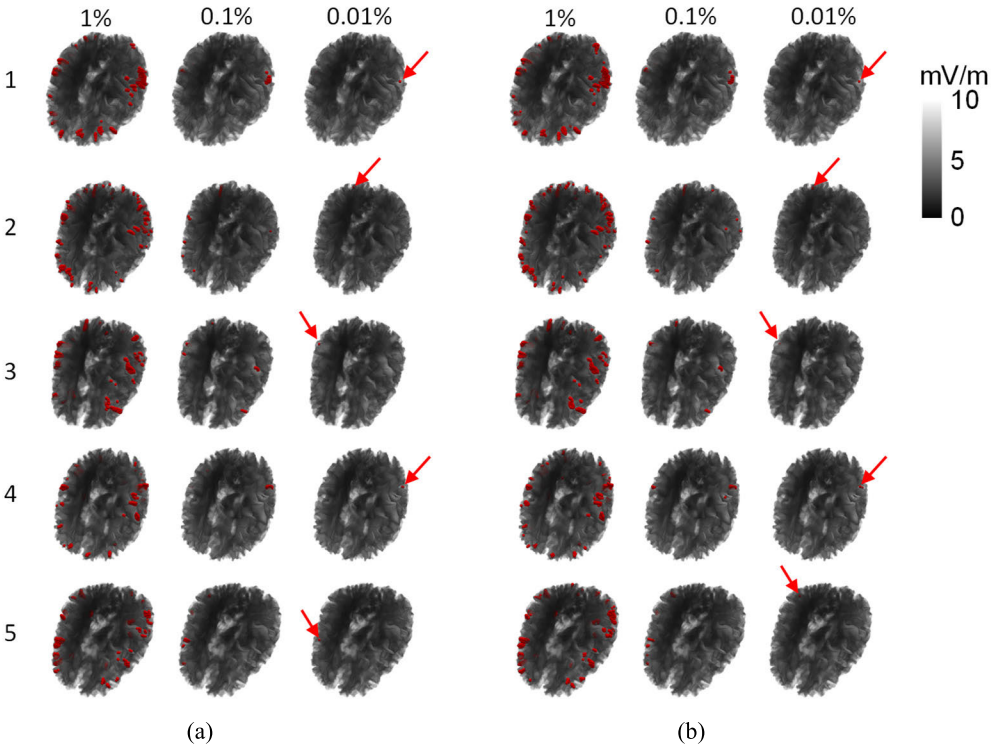

FIGURE 9. Locations of the top 1% to 0.01% of the averaged electric field strengths in WM for (a) method 1 and (b) method 2, respectively.

evaluated for GM and WM. Due to the similarity in the results, data from one group were reported. The results for model no. 1 are presented in Figs. 6 (a) and (b) for the two averaging methods. As can be seen, when $p_{\max} = 0\%$, due to the thickness and complex anatomy of GM, a considerable portion of the voxels of GM was excluded. The number of excluded voxels gradually decreases as more nontarget tissue is allowed in the cube.

The percentile values of the averaged electric field in the WM of five nonuniform head models for different $p_{\max}$ are presented in Fig. 7. When $p_{\max} > 20\%$, the percentile values become stable for various values of $p_{\max}$. At $p_{\max} = 40\%$, the highest 99.99^{th} percentile values among the five head modes are 8.4 and 7.8 mV/m for methods 2 and 1, respectively; the highest 99.9^{th} percentile value among the five models is about 6.5 mV/m for both methods.

As can be seen from Fig. 7, the 99th to 99.99th percentile values in the WM are generally consistent for methods 1 and 2. However, the tendencies for the 100th percentile values are different. The percentage of other tissues inside the cube does not significantly affect the averaged electric field even for the 100th percentile values for method 1. While for method 2, the 100th percentile value increases with p_{max}. This is because for method 1, the averaging volume includes the neighboring GM voxels, and the electric field across the GM/WM interface does not significantly differ due to the smooth transition of the conductivity. For method 2, averaging is performed only with the target tissue; a higher p_{max} indicates reduced averaging volume, hence higher averaged 100th percentile values.

The percentile values for GM are presented in Figs. 8 (a) and (b) for methods 1 and 2, respectively. Except for the 100th percentile value, the 99th to 99.99th percentile values for the five head models are generally consistent. Method 1 generally has higher 100th percentile values due to the inclusion of higher electric field strengths in WM in the averaging volume. The electric field strengths in GM are lower than those in the WM, which is attributed to the conductivity of the outermost layers of the GM voxels being affected by the high-conductivity CSF for the learning-based models. Similar tendencies were also observed at 10 kHz (results not shown).

D. LOCATIONS OF THE TOP 1% ELECTRIC FIELD STRENGTHS IN THE WM

Fig. 9 presents the locations of the top 1% averaged electric field strengths on the head models for the two cubic averaging methods at 50 Hz. The highest electric field strengths generally appear at voxels in the gyruses of the WM. Furthermore, the locations of the top 1%–0.01% electric field strengths illustrate the consistency of two cubic averaging methods for electric fields in WM. Due to the low contrast in the conductivity between WM and GM, and the smooth conductivity transition in the learning-based models, staircasing artifacts are not significant for WM. Thus, as has been demonstrated in several previous studies [27], [43], the 99th or higher percentile values may exclude voxels with actual high electric field strengths for head exposure to a uniform LF magnetic field.

E. ELECTRIC FIELD IN THE SKIN

Fig. 10 presents the distributions of conductivity and resultant electric field strength in the border skin voxels of model no. 1. As can be seen from Fig. 10 (a), as mapped directly from the medical images, the skin conductivities at the border voxel reflect the volume fraction of the skin tissue within the border voxel. A previous study demonstrated that considering the partial volume effect reduces staircasing errors [45]. Therefore, staircasing artifacts on boundary skin voxel were suppressed, as can be seen from Fig. 10 (b). This is an advantage of the use of learning-based nonuniform models for dosimetry. However, the artifacts in some parts of the skin

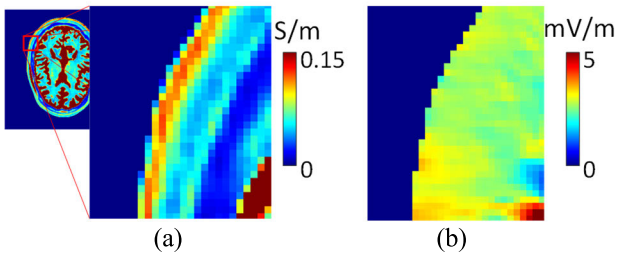

FIGURE 10. Distributions of (a) conductivity and (b) electric field strength on skin voxels for model no. 1 at 50 Hz.

voxels were not notably reduced due to the noise in medical images attributed to the instrument signal-to-noise ratio and the movement of the subject during the imaging process.

IV. DISCUSSION AND CONCLUDING REMARKS

The intercomparison of the electric field cubically averaged over 8 mm^3 (2 mm × 2 mm × 2 mm) in the head models for exposure to an LF magnetic field was coordinated under a working group of Subcommittee 6 of IEEE ICES Technical Committee 95. This study aimed to derive an appropriate reduction factor, which is needed to set the limit in exposure guidelines and study. For this purpose, a novel learning-based head model was used for the first time in the intercomparison for the assessment of LF magnetic field exposures. The computational conditions were harmonized as much as possible, and a high degree of consistency across seven research groups have been reported for both frequencies, being $<1\%$ for most cases.

The highest RD was found to be 23% between the use of the SPFD method and FEM. A possible explanation for this fact is that the employed FEM formulation is equivalent to a minimization problem for the total coenergy of the system, which has to be numerically approximated. Due to the unavoidable errors caused by discretization, the computed coenergy is an approximation that overestimates the true coenergy [38]. Hence, one expects that in average, the electric field strength numerically computed by using this formulation is higher than the exact electric field. However, notice that this result does not hold locally – that is, in a minority of points, the numerically computed electric field can be lower than the exact electric field, even if, in average, it is bound to be higher. In [38], a different formulation was also reported, which underestimates the energy, but it has not been used in this work.

The RDs in the electric field computed using the SPFD method with different solvers are generally below 1%, except for one group. These RDs are generally lower compared with the previous intercomparison studies: ∼200% in [28], ∼10% or higher reported in [29], and ∼5% in [30]. As can be seen, the computational uncertainties caused by the codes can be reduced for a clearly defined model and exposure condition. Several main reasons contribute to the consistency: 1), nonuniform conductivity reduced the staircasing error, which is the main source of the computational uncertainty;

2) although different solvers were used, most groups used the six-point scheme of the SPFD method, and all computations met the same stop criterion; and 3) the head models used here do not have skin-to-skin contact region, which may emphasize the uncertainty [30].

The peak electric field strengths in the WM are higher than that in the GM for the models used here. In [46], the electric field in the WM was higher than that in the GM in 17% of cases for TOP exposure. This is because for the learning-based models, the conductivity values of several outermost layers of voxels in the GM were higher than the uniform conductivity values of the GM of segmented models. Because the conductivity contrast between the GM and WM is lower than that between the GM and CSF, the induced electric field does not significantly differ across the GM/WM interface. This is the cause of the stable 100th percentile values of the electric field averaged using method 1 in WM (Fig. 7) regardless of the inclusion ratio of other tissues in the averaging volume.

The highest 99th and 100th percentile values in the WM for method 1 are ∼5 and ∼9 mV/m, respectively, for 200-μT external magnetic field at 50 Hz, corresponding to ∼25 and ∼45 mV/m per mT. The 99th percentile electric fields in the brain computed in [4] were 25.1 and 22.1 mV/m per mT in the NAOMI and NORMAN models, respectively, for the magnetic field in the TOP direction. The 99th percentile values in WM also agree with those in [47], which were 22.9 and 20.1 mV/m per mT in the brains of the TARO and HANAKO models, respectively. In the IEEE standard [1], magnetic induction was computed using homogeneous ellipsoidal models. For the exposure of the ellipsoid to a magnetic field at 50 Hz, the induced electric field can be calculated to be about 16.3 mV/m per mT. This value is lower than the value in this study as only a homogeneous canonical model was considered [48]. The 99th percentile values were used to suppress the effect of staircasing representation of the curved tissue boundaries. Some studies have suggested that a percentile value of about 99.99th of the averaged electric field strength can be used as a representative value of the actual peak if the staircasing error has been reduced (..) [16], [27]. In our case, though not perfectly, the nonuniform model itself suppressed the staircasing error to some degree based on the inherent incorporation of the volume fraction of tissue within the voxel, as directly mapped from the medical image gray level (Fig. 10). Note that the 99th percentile is applied to the body model, not in the head. In the body model, the induced electric field becomes high around the armpit, inseam, etc., because of the modeling there, which is different from the head model. Thus, a direct conclusion cannot be derived from this study.

In conclusion, the uncertainty caused by the different computational codes was much reduced by considering a learning-based head model in which a smooth transition of the conductivity is replicated. Even when the maximum value of the spatially averaged electric field was considered, the relative difference was 23%, which is much smaller than the reduction factor of 3. This finding may help in setting an appropriate reduction factor and the exposure limit in future revisions of international guidelines and standards. In future work, we will consider a learning method that derives the anisotropic conductivity of tissues, such as the nerves and muscles, improve the numerical method for the estimation of the exposure dose in such models, and assess the effect of anisotropic conductivities on the maximum exposure dose.

APPENDIX

The source code of CondNet is available in Mathematica (https://github.com/erashed/CondNet) and Python (https://github.com/rrwabina/condnet).

ACKNOWLEDGMENT

The authors would like to thank Dr. Kensuke Sasaki (National Institute of Information and Communications Technology, Tokyo, Japan) for valuable discussion on tissue dielectric properties and support for working group activities.

REFERENCES

[1] *IEEE Standard for Safety Levels With Respect to Human Exposure to Electric, Magnetic and Electromagnetic Fields*, Standard IEEE-C95.1, 2019.

[2] International Commission on Non-Ionizing Radiation Protection, "Guidelines for limiting exposure to Electromagnetic Fields (100 kHz to 300 GHz)," *Health Phys.*, vol. 118, no. 5, pp. 483–524, May 2020, doi: 10.1097/hp.0000000000001210.

[3] International Commission on Non-Ionizing Radiation Protection, "Guidelines for limiting exposure to time-varying electric and magnetic fields (1 Hz to 100 kHz)," *Health Phys.*, vol. 99, no. 6, pp. 818–836, 2010, doi: 10.1097/HP.0b013e3181f06c86.

[4] P. Dimbylow, "Development of the female voxel phantom, NAOMI, and its application to calculations of induced current densities and electric fields from applied low frequency magnetic and electric fields," *Phys. Med. Biol.*, vol. 50, no. 6, pp. 1047–1070, Mar. 2005, doi: 10.1088/0031-9155/50/6/002.

[5] A. Hirata, Y. Diao, T. Onishi, K. Sasaki, S. Ahn, D. Colombi, V. De Santis, I. Laakso, L. Giaccone, W. Joseph, and E. A. Rashed, "Assessment of human exposure to electromagnetic fields: Review and future directions," *IEEE Trans. Electromagn. Compat.*, vol. 63, no. 5, pp. 1619–1630, Oct. 2021, doi: 10.1109/TEMC.2021.3109249.

[6] J. P. Reilly and A. Hirata, "Low-frequency electrical dosimetry: Research agenda of the IEEE international committee on electromagnetic safety," *Phys. Med. Biol.*, vol. 61, no. 12, pp. 138–149, Jun. 2016, doi: 10.1088/0031-9155/61/12/R138.

[7] International Commission on Non-Ionizing Radiation Protection, "Gaps in knowledge relevant to the 'guidelines for limiting exposure to time-varying electric and magnetic fields (1 Hz-100 kHz),'" *Health Phys.*, vol. 118, no. 5, pp. 533–542, 2020, doi: 10.1097/HP.0000000000001261.

[8] S. Gabriel, R. W. Lau, and C. Gabriel, "The dielectric properties of biological tissues: III. Parametric models for the dielectric spectrum of tissues," *Phys. Med. Biol.*, vol. 41, no. 11, pp. 2271–2293, 1996, doi: 10.1088/0031-9155/41/11/003.

[9] K. Sasaki, E. Porter, E. A. Rashed, L. Farrugia, and G. Schmid, "Measurement and image-based estimation of dielectric properties of biological tissues—Past, present, and future," *Phys. Med. Biol.*, vol. 67, no. 14, Jul. 2022, Art. no. 14TR01, doi: 10.1088/1361-6560/ac7b64.

[10] T. W. Dawson, K. Caputa, and M. A. Stuchly, "High-resolution organ dosimetry for human exposure to low-frequency electric fields," *IEEE Trans. Power Del.*, vol. 13, no. 2, pp. 366–373, Apr. 1998, doi: 10.1109/61.660903.

[11] A. Hirata, K. Caputa, T. W. Dawson, and M. A. Stuchly, "Dosimetry in models of child and adult for low-frequency electric field," *IEEE Trans. Biomed. Eng.*, vol. 48, no. 9, pp. 1007–1012, Sep. 2001, doi: 10.1109/10.942590.

[12] P. J. Dimbylow, "Induced current densities from low-frequency magnetic fields in a 2 mm resolution, anatomically realistic model of the body," *Phys. Med. Biol.*, vol. 43, no. 2, pp. 221–230, Feb. 1998, doi: 10.1088/0031-9155/43/2/001.
[13] K. Caputa, P. J. Dimbylow, T. W. Dawson, and M. A. Stuchly, "Modelling fields induced in humans by 50/60 Hz magnetic fields: Reliability of the results and effects of model variations," *Phys. Med. Biol.*, vol. 47, no. 8, pp. 1391–1398, Apr. 2002, doi: 10.1088/0031-9155/47/8/311.
[14] C. Li and T. Wu, "Dosimetry of infant exposure to power-frequency magnetic fields: Variation of 99th percentile induced electric field value by posture and skin-to-skin contact," *Bioelectromagnetics*, vol. 36, no. 3, pp. 204–218, 2015, doi: 10.1002/bem.21899.
[15] R. P. Findlay, "Induced electric fields in the MAXWEL surface-based human model from exposure to external low frequency electric fields," *Radiat. Protection Dosimetry*, vol. 162, no. 3, pp. 244–253, Dec. 2014, doi: 10.1093/rpd/nct281.
[16] X.-L. Chen, S. Benkler, N. Chavannes, V. De Santis, J. Bakker, G. Van Rhoon, J. Mosig, and N. Kuster, "Analysis of human brain exposure to low-frequency magnetic fields: A numerical assessment of spatially averaged electric fields and exposure limits," *Bioelectromagnetics*, vol. 34, no. 5, pp. 375–384, Jul. 2013, doi: 10.1002/bem.21780.
[17] G. Schmid and R. Hirtl, "On the importance of body posture and skin modelling with respect toin situelectric field strengths in magnetic field exposure scenarios," *Phys. Med. Biol.*, vol. 61, no. 12, pp. 4412–4437, May 2016, doi: 10.1088/0031-9155/61/12/4412.
[18] Y. Takahashi, A. Ahagon, K. Fujiwara, T. Iwashita, and H. Nakashima, "Analysis of induced electric field in human body by utility power frequency magnetic field using parallel fast multipole-accelerated boundary element method," *IET Sci., Meas. Technol.*, vol. 9, no. 2, pp. 178–183, Mar. 2015, doi: 10.1049/iet-smt.2014.0195.
[19] I. Liorni, M. Parazzini, S. Fiocchi, M. Douglas, M. Capstick, M.-C. Gosselin, N. Kuster, and P. Ravazzani, "Dosimetric study of fetal exposure to uniform magnetic fields at 50 Hz," *Bioelectromagnetics*, vol. 35, no. 8, pp. 580–597, Dec. 2014, doi: 10.1002/bem.21878.
[20] K. Taguchi, I. Laakso, K. Aga, A. Hirata, Y. Diao, J. Chakarothai, and T. Kashiwa, "Relationship of external field strength with local and whole-body averaged specific absorption rates in anatomical human models," *IEEE Access*, vol. 6, pp. 70186–70196, 2018, doi: 10.1109/ACCESS.2018.2880905.
[21] J. Chakarothai, K. Wake, T. Arima, S. Watanabe, and T. Uno, "Exposure evaluation of an actual wireless power transfer system for an electric vehicle with near-field measurement," *IEEE Trans. Microw. Theory Techn.*, vol. 66, no. 3, pp. 1543–1552, Mar. 2018, doi: 10.1109/TMTT.2017.2748949.
[22] T. Campi, S. Cruciani, V. De Santis, F. Maradei, and M. Feliziani, "EMC and EMF safety issues in wireless charging system for an electric vehicle (EV)," in *Proc. Int. Conf. Electr. Electron. Technol. for Automot.*, Jun. 2017, pp. 1–4, doi: 10.23919/EETA.2017.7993214.
[23] S. Hong, I. Cho, H. Choi, and J. Pack, "Numerical anlaysis of human exposure to electromagnetic fields from wireless power transfer systems," in *Proc. IEEE Wireless Power Transf. Conf.*, May 2014, pp. 216–219, doi: 10.1109/WPT.2014.6839587.
[24] K. Wake, I. Laakso, A. Hirata, J. Chakarothai, T. Onishi, S. Watanabe, V. De Santis, M. Feliziani, and M. Taki, "Derivation of coupling factors for different wireless power transfer systems: Inter- and intralaboratory comparison," *IEEE Trans. Electromagn. Compat.*, vol. 59, no. 2, pp. 677–685, Apr. 2017, doi: 10.1109/TEMC.2016.2636328.
[25] A. Arduino, O. Bottauscio, M. Chiampi, L. Giaccone, I. Liorni, N. Kuster, L. Zilberti, and M. Zucca, "Accuracy assessment of numerical dosimetry for the evaluation of human exposure to electric vehicle inductive charging systems," *IEEE Trans. Electromagn. Compat.*, vol. 62, no. 5, pp. 1939–1950, Oct. 2020, doi: 10.1109/TEMC.2019.2954111.
[26] A. C. Gubernati, F. Freschi, L. Giaccone, and R. Scorretti, "Analysis of numerical artifacts using tetrahedral meshes in low frequency numerical dosimetry," *Appl. Sci.*, vol. 12, no. 13, p. 6526, 2022, doi: 10.3390/app12136526.
[27] M. Soldati and I. Laakso, "Computational errors of the induced electric field in voxelized and tetrahedral anatomical head models exposed to spatially uniform and localized magnetic fields," *Phys. Med. Biol.*, vol. 65, no. 1, Jan. 2020, Art. no. 015001, doi: 10.1088/1361-6560/ab5dfb.
[28] M. A. Stuchly and O. P. Gandhi, "Inter-laboratory comparison of numerical dosimetry for human exposure to 60 Hz electric and magnetic fields," *Bioelectromagnetics*, vol. 21, no. 3, pp. 167–174, Apr. 2000, doi: 10.1002/(SICI)1521-186X(200004)21:3<167:AID-BEM3>3.0.CO;2-1.
[29] A. Hirata, K. Yamazaki, S. Hamada, Y. Kamimura, H. Tarao, K. Wake, Y. Suzuki, N. Hayashi, and O. Fujiwara, "Intercomparison of induced fields in Japanese male model for ELF magnetic field exposures: Effect of different computational methods and codes," *Radiat. Protection Dosimetry*, vol. 138, no. 3, pp. 237–244, Nov. 2010, doi: 10.1093/rpd/ncp251.
[30] K. Aga, A. Hirata, I. Laakso, H. Tarao, Y. Diao, T. Ito, Y. Sekiba, and K. Yamazaki, "Intercomparison of in situ electric fields in human models exposed to spatially uniform magnetic fields," *IEEE Access*, vol. 6, pp. 70964–70973, 2018, doi: 10.1109/ACCESS.2018.2881277.
[31] E. A. Rashed, J. Gomez-Tames, and A. Hirata, "Deep learning-based development of personalized human head model with non-uniform conductivity for brain stimulation," *IEEE Trans. Med. Imag.*, vol. 39, no. 7, pp. 2351–2362, Jul. 2020, doi: 10.1109/tmi.2020.2969682.
[32] Y. Diao, E. A. Rashed, and A. Hirata, "Induced electric field in learning-based head models with smooth conductivity for exposure to uniform low-frequency magnetic fields," *IEEE Trans. Electromagn. Compat.*, vol. 64, no. 6, pp. 1969–1977, Dec. 2022, doi: 10.1109/TEMC.2022.3212860.
[33] *MIDAS—Collection NAMIC: Brain Mutlimodality*. Accessed: Apr. 22, 2020. [Online]. Available: http://insight-journal.org/midas/collection/view/190
[34] E. A. Rashed, J. Gomez-Tames, and A. Hirata, "Development of accurate human head models for personalized electromagnetic dosimetry using deep learning," *NeuroImage*, vol. 202, Nov. 2019, Art. no. 116132, doi: 10.1016/j.neuroimage.2019.116132.
[35] A. Hirata, F. Ito, and I. Laakso, "Confirmation of quasi-static approximation in SAR evaluation for a wireless power transfer system," *Phys. Med. Biol.*, vol. 58, no. 17, pp. 241–249, 2013, doi: 10.1088/0031-9155/58/17/N241.
[36] A. Barchanski, H. D. Gersem, E. Gjonaj, and T. Weiland, "Impact of the displacement current on low-frequency electromagnetic fields computed using high-resolution anatomy models," *Phys. Med. Biol.*, vol. 50, no. 19, pp. 243–249, Oct. 2005, doi: 10.1088/0031-9155/50/19/n02.
[37] S. W. Park, K. Wake, and S. Watanabe, "Calculation errors of the electric field induced in a human body under quasi-static approximation conditions," *IEEE Trans. Microw. Theory Techn.*, vol. 61, no. 5, pp. 2153–2160, May 2013, doi: 10.1109/TMTT.2013.2247211.
[38] R. Scorretti, R. V. Sabariego, L. Morel, C. Geuzaine, N. Burais, and L. Nicolas, "Computation of induced fields into the human body by dual finite element formulations," *IEEE Trans. Magn.*, vol. 48, no. 2, pp. 783–786, Feb. 2012, doi: 10.1109/TMAG.2011.2174037.
[39] F. Freschi, L. Giaccone, V. Cirimele, and A. Canova, "Numerical assessment of low-frequency dosimetry from sampled magnetic fields," *Phys. Med. Biol.*, vol. 63, no. 1, Dec. 2017, Art. no. 015029, doi: 10.1088/1361-6560/aa9915.
[40] Y. Notay, "An aggregation-based algebraic multigrid method," *Electron. Trans. Numer. Anal.*, vol. 37, pp. 123–146, Oct. 2010.
[41] I. Laakso and A. Hirata, "Fast multigrid-based computation of the induced electric field for transcranial magnetic stimulation," *Phys. Med. Biol.*, vol. 57, no. 23, pp. 7753–7765, 2012, doi: 10.1088/0031-9155/57/23/7753.
[42] Y. Diao, J. Gomez-Tames, E. A. Rashed, R. Kavet, and A. Hirata, "Spatial averaging schemes of in situ electric field for low-frequency magnetic field exposures," *IEEE Access*, vol. 7, pp. 184320–184331, 2019, doi: 10.1109/ACCESS.2019.2960394.
[43] J. Gomez-Tames, I. Laakso, Y. Haba, A. Hirata, D. Poljak, and K. Yamazaki, "Computational artifacts of the in situ electric field in anatomical models exposed to low-frequency magnetic field," *IEEE Trans. Electromagn. Compat.*, vol. 60, no. 3, pp. 589–597, Jun. 2018, doi: 10.1109/TEMC.2017.2748219.
[44] I. Laakso and A. Hirata, "Reducing the staircasing error in computational dosimetry of low-frequency electromagnetic fields," *Phys. Med. Biol.*, vol. 57, no. 4, pp. 25–34, 2012, doi: 10.1088/0031-9155/57/4/N25.
[45] Y. Diao, L. Zhang, D. Shi, and A. Hirata, "An effective edge conductivity for reducing staircasing error in induced electric field computation for low-frequency magnetic field dosimetry," *Phys. Med. Biol.*, vol. 67, no. 21, Oct. 2022, Art. no. 215011, doi: 10.1088/1361-6560/ac944b.
[46] M. Soldati, T. Murakami, and I. Laakso, "Inter-individual variations in electric fields induced in the brain by exposure to uniform magnetic fields at 50 Hz," *Phys. Med. Biol.*, vol. 65, no. 21, Oct. 2020, Art. no. 215006, doi: 10.1088/1361-6560/aba21e.
[47] A. Hirata, K. Wake, S. Watanabe, and M. Taki, "In-situ electric field and current density in Japanese male and female models for uniform magnetic field exposures," *Radiat. Prot. Dosimetry*, vol. 135, no. 4, p. 272, 2009, doi: 10.1093/rpd/ncp117.

[48] A. Hirata, Y. Takano, O. Fujiwara, T. Dovan, and R. Kavet, "An electric field induced in the retina and brain at threshold magnetic flux density causing magnetophosphenes," *Phys. Med. Biol.*, vol. 56, no. 13, pp. 4091–4101, Jun. 2011, doi: 10.1088/0031-9155/56/13/022.

YINLIANG DIAO (Member, IEEE) received the B.E. degree from Chongqing University, Chongqing, China, in 2008, the M.S. degree in electronic engineering from the Beijing University of Posts and Telecommunications, Beijing, China, in 2011, and the Ph.D. degree in electronic engineering from the City University of Hong Kong, in 2016. Since 2017, he has been an Assistant Professor with South China Agricultural University, Guangzhou, China. From 2019 to 2021, he was a Research Assistant/an Associate Professor with the Nagoya Institute of Technology, where he is currently a Guest Associate Professor. His current research interests include electromagnetic dosimetry modeling and electromagnetic compatibility. He is a member of IEEE ICES Standards Coordinating Committee and the Scientific Expert Group of International Commission on Non-Ionizing Radiation Protection. He was a recipient of the Young Scientist Award from URSI GASS 2020.

ESSAM A. RASHED (Senior Member, IEEE) received the Ph.D. (Eng.) degree in computer science from the University of Tsukuba, Tsukuba, Japan, in 2010. From 2010 to 2012, he was a JSPS Research Fellow with the University of Tsukuba. He served as an Assistant/Associate/Full Professor of computer science with the Department of Mathematics, Faculty of Science, Suez Canal University. From 2018 to 2021, he was a Research Professor with the Nagoya Institute of Technology, Japan. He is currently a Professor with the Graduate School of Information Science, University of Hyogo, Kobe, Japan. His research interests include medical image processing, data science, artificial intelligence, and pattern recognition. He was a recipient of the Egyptian National Doctoral Scholarship, in 2006; the JSPS Postdoctoral Fellowship, in 2010; the JAMIT Best Presentation Award, in 2008 and 2012; and the Chairman Award from the Department of Computer Science, University of Tsukuba, in 2010. He has participated as a PI and a Co-I for several external funded projects. He is an Associate Editor of IEEE Access.

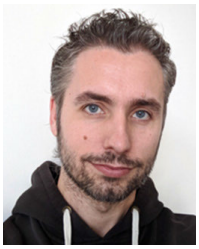

LUCA GIACCONE (Senior Member, IEEE) was born in Cuneo, Italy, in 1980. He received the Laurea and Ph.D. degrees in electrical engineering from Politecnico di Torino, Turin, Italy, in 2005 and 2010, respectively. He works on several areas of the electrical engineering, such as optimization, modeling of complex energy systems, computation of electromagnetic and thermal fields, energy scavenging, magnetic field mitigation, EMF dosimetry, and compliance of LF pulsed magnetic field sources. Since 2017, he has been an Associate Professor with Dipartimento Energia "G: Ferraris," Politecnico di Torino. Since 2015, he has been a member of the IEEE International Committee on Electromagnetic Safety—Technical Committee 95–SC6–dosimetry modeling. Since September 2017, he has been a member of the National Italian Committee CEI-106 dealing with human exposure to electromagnetic fields. In 2020, he was appointed as a member of the ICNIRP Scientific Expert Group (SEG).

ILKKA LAAKSO (Member, IEEE) received the M.Sc. (Tech.) degree in electromagnetics and circuit theory from the Helsinki University of Technology, Espoo, Finland, in 2007, and the D.Sc. (Tech.) degree in electromagnetics from Aalto University, Espoo, in 2011. From 2013 to 2015, he was a Research Assistant Professor and a Research Associate Professor with the Department of Computer Science and Engineering, Nagoya Institute of Technology. Since 2015, he has been an Assistant Professor with Aalto University, where he has been an Associate Professor, since 2023. He is the author of more than 100 papers published in international journals and conference proceedings. His research interests include computational bioelectromagnetic modeling for assessment of human safety and biomedical applications. He is a member of the IEEE International Committee on Electromagnetic Safety and the Scientific Expert Group of the International Commission on Non-Ionizing Radiation. He received several awards, including the Ericsson Young Scientist Award, in 2011; the Young Scientist Award in URSI General Assembly and Scientific Symposium, Montreal, Canada, in 2017; and the IEEE Electromagnetic Compatibility Society Technical Achievement Award for contribution to computational dosimetry of human exposure to electromagnetic fields from low frequencies to millimeter waves, in 2021.

CONGSHENG LI received the B.S. degree in electronic information engineering from Beijing City University, Beijing, China, in 2009, the M.S. degree in signal and information system from Beijing Information Science and Technology University, Beijing, in 2012, and the Ph.D. degree from the University of Science and Technology Beijing, China, in 2015. Since 2015, he has been an Engineer and a Senior Engineer with the China Academy of Information and Communications Technology, Beijing. His research interests include computational electromagnetics and artificial intelligence.

RICCARDO SCORRETTI was born in Prato, Italy, in 1973. He received the Laurea (aka M.S. degree) degree in informatics engineering from Florence University, Italy, in 1999, and the Ph.D. degree in electrical engineering from Ecole Centrale de Lyon, France, in 2003. In 2005, he joined the National Council of Scientific Research, Laboratoire Ampère–UMR 5005 CNRS, Lyon, France. In 2009 and 2019, he was a Visiting Scientist with Institut Montefiore, University of Liège, Belgium; and the Nagoya Institute of Technology, Japan, respectively. He is currently a Visiting Scientist with the University of Perugia, Italy. His research focus on computational electromagnetism, including modeling of hysteresis in magnetic materials and numerical dosimetry of electromagnetic fields. Since 2022, he has been a member of the IEEE International Committee on Electromagnetic Safety—Technical Committee 95–SC6–dosimetry modeling.

YOICHI SEKIBA (Member, IEEE) received the B.S. and M.S. degrees in physics from Tohoku University, Sendai, Japan, in 2008 and 2010, respectively. In 2010, he joined the Denryoku Computing Center, Komae, Tokyo, Japan. From 2013 to 2016, he was a temporary Assignment Researcher with the Central Research Institute of Electric Power Industry (CRIEPI), Yokosuka, Kanagawa, Japan. His current research interest includes evaluation of human exposure to electromagnetic field by numerical EMF analysis. His research interest also includes analysis of power systems by electromagnetic transient simulations. He is a member of IEE Japan.

KENICHI YAMAZAKI (Senior Member, IEEE) was born in Yokohama, Japan, in February 1968. He received the B.S. degree in applied physics from the Tokyo University of Science, Tokyo, Japan, in 1990, and the M.S. and Ph.D. degrees in biomedical engineering from Hokkaido University, Sapporo, Japan, in 1992 and 2001, respectively. In 1992, he joined the Central Research Institute of Electric Power Industry (CRIEPI), Yokosuka, Tokyo, where he is currently the Deputy Head of the Electric Facility Technology Division. From 2002 to 2003, he was a Visiting Scientist with the School of Electrical Engineering and Computer Science, Washington State University, Pullman, WA, USA. His research interests include the characterization of human exposure to low-frequency electromagnetic fields and power line electromagnetic compatibility. He is a member of the Bioelectromagnetics Society and a Senior Member of IEE Japan.

AKIMASA HIRATA (Fellow, IEEE) received the B.E., M.E., and Ph.D. degrees in communications engineering from Osaka University, Suita, Japan, in 1996, 1998, and 2000, respectively. From 1999 to 2001, he was a Research Fellow with the Japan Society for the Promotion of Science. He was a Visiting Research Scientist with the University of Victoria, Victoria, BC, Canada, in 2000. In 2001, he joined the Department of Communications Engineering, Osaka University, as an Assistant Professor. In 2004, he joined as an Associate Professor with the Department of Computer Science and Engineering, Nagoya Institute of Technology, where he is currently a Full Professor. His research interests include electromagnetic safety, risk management system for heat-related illness, methods in neuroscience, antennas, filters, and related computational techniques. He is an editorial board member of physics in medicine and biology, a member of the main commission and the Chair of project group of International Commission on Non-Ionizing Radiation Protection, and a member of administrative committee and a Subcommittee (EMF Dosimetry Modeling) Chair of IEEE International Committee on Electromagnetic Safety, and an Expert of World Health Organization. From 2006 to 2012, he was an Associate Editor of the IEEE TRANSACTIONS ON BIOMEDICAL ENGINEERING. He received several awards, including the Young Scientists' Prize in 2006 and the Prizes for Science and Technology (Research Category in 2011, Public Understanding Promotion Category in 2014, 2020) by the Commendation for Science and Technology by the Minister of Education, Culture, Sports, Science, and Technology, Japan, the IEEE EMC-S Technical Achievement Award (2015), the Japan Academy Medal and JSPS Prize in 2018, and the Japan Open Innovation Prize (President of the Science Council of Japan Prize in 2022) from the Cabinet Office. He is a fellow of Institute of Physics and a member of IEICE, IEE Japan, and Bioelectromagnetics Society.